ACS OMEGA

Open Access

http://pubs.acs.org/journal/acsodf

Article

Optimizations of Liquid Phase Deposition Processes for Enhanced Photoelectrocatalytic Activities of Tungsten Oxide Thin Films

Watcharapong Nareejun, Chatchai Ponchio,* Minoru Mizuhata, and Hiro Minamimoto*

Cite This: *ACS Omega* 2024, 9, 38788−38797

Read Online

ACCESS | Metrics & More | Article Recommendations | Supporting Information

ABSTRACT: This study focuses on the preparation of tungsten oxide (WO_3) as the photoanode for water oxidations by the liquid phase deposition (LPD) technique and its optimizations to improve the photoelectrochemical performance. The alternative precursor large stock solution process was achieved to simplify the LPD process for WO_3 thin film preparation. The effect of boric acid in the precursor solutions on the physicochemical properties of the deposited WO_3 thin films was investigated. As a result, we found that the optimized concentration of boric acid realized the highest photoelectrochemical performance. Through the optimizations of reaction conditions and surface analyses, we concluded that the preparations of a semiconductor film via the LPD technique had the potential to obtain high-performance photoelectrocatalytic applications.

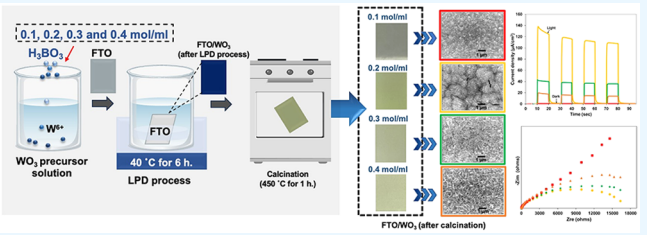

1. INTRODUCTION

The photoelectrocatalytic (PEC) technology has gained considerable interest in energy and environmental applications because of its notable efficiency, affordability, simplicity, and ecologically sustainable characteristics.[1−3] The development of PEC systems relies heavily on appropriate semiconductor materials, particularly metal oxide semiconductors. Researchers are investigating many metal oxide semiconductors, such as TiO_2,[4−6] $BiVO_4$,[7,8] Fe_2O_3,[9,10] Cr_2O_3,[11] $CuYO_2$,[12] Mn_2O_3,[13] or WO_3,[14,15] as photoanodes for water oxidation because of their exceptional performance and durability. Especially, WO_3 would be promising in converting visible-light energy due to its excellent efficiency and stability,[16] as well as its narrow band gap energy ranging between 2.4−2.8 eV.[17] In addition, the valence band (VB) of WO_3 has a more positive potential, which is favorable for promoting high-energy oxidation processes. WO_3 is often employed alone or in combination with other semiconductors like $BiVO_4$[18] or composites like Pt/WO_3−C.[19] The approach of depositing the WO_3 film onto the support material substantially impacts and enhances the photoelectrocatalytic oxidation reactions. Various methods of WO_3 thin film fabrication have been employed to improve the PEC efficiency. The spin coating, sputtering, electrodeposition, and liquid phase deposition (LPD) are among the deposition techniques utilized. The structural, morphological, and PEC characteristics of WO_3 films are affected differently by each process. Electrodeposition has the ability to produce films that demonstrate outstanding uniformity and adherence.[20] Conversely, sputtering allows for the creation of films that have exceptionally high levels of purity and exact control over their thickness.[21] The spin coating[22] and LPD[23,24] methods are widely favored for their cost-effectiveness and ease of usage in achieving crystallographic organization and film formation. Moreover, these two methods provide significant advantages. Therefore, it is essential to develop a method for fabricating the WO_3 film that ensures the operations' simplicity and cost-effectiveness and improves the adhesion between the thin film and the substrate.

The LPD is an attractive technique due to its inherent simplicity, the strong adhesion to the substrate, and lack of need for expensive equipment.[25,26] Until now, we have established various types of LPD processes based on the slow hydrolysis of the fluorine metal complex species, leading to high-quality metal oxide films.[27−29] Not only for our reports but also for other studies, it is known that the slow hydrolysis of W-fluoro complexes in the presence of boric acid and a fluoride scavenger can achieve WO_3 film preparations.[30,31] In the LPD reaction solutions, boric acid promotes uniform nucleation and growth of WO_3 crystals on the substrate surface while keeping the crystallinity of deposits. The significance of boric acid in controlling the quality and efficiency of WO_3 thin film fabricated by the LPD technique was highlighted in the previous report.[30] However, there are few reports of in-depth studies about the precursor solution preparation method and the effect of boric acid on the quality of WO_3 in the PEC

Received: May 19, 2024
Revised: August 14, 2024
Accepted: August 19, 2024
Published: September 4, 2024

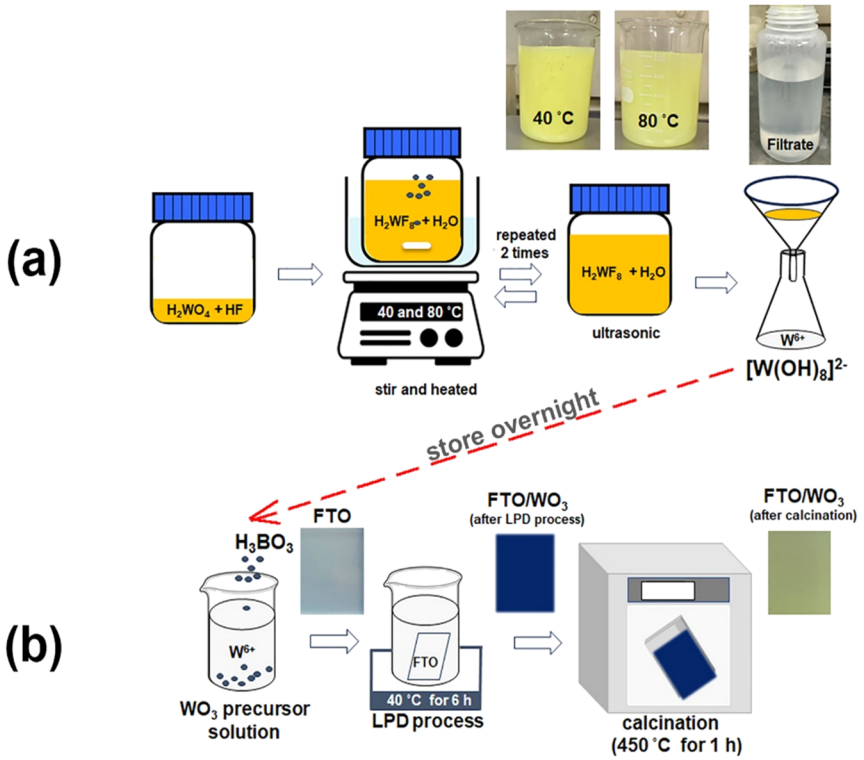

Figure 1. Schematic diagram of WO_3 thin film fabrication by the LPD process. (a) WO_3 precursor solution preparation step and (b) LPD deposition step and calcination process.

water-splitting process. These insights would greatly influence the performance of the PEC process.

From the above backgrounds, this research focuses on the preparation procedure of the precursor solution and the effect of boric acid on the performance of the WO_3 thin film as the photoanode in the PEC cell. As a result, we successfully found the optimized concentration of boric acid in the precursor solution to achieve efficient water oxidation reactions in the PEC process. The outstanding results of the study were that we obtained a well-homogenized precursor solution in a shorter time and were able to significantly increase the efficiency of immobilizing the WO_3 film to the substrate. The impact of boric acid on the distinctive features and PEC capabilities of a WO_3 photoanode can be comprehensively elucidated in the reaction. The findings would have a significant impact on the advancement of the LPD technique as the fabrication process of the highly efficient electrode for PEC applications.

2. EXPERIMENTAL SECTION

2.1. Fabrication of a WO_3 Photoanode by the LPD Process. Figure 1a illustrates the preparation procedure of the parent solution of the W-fluorine species. 1.25 g of tungstic acid (H_2WO_4; SIGMA-Aldrich) powder was added to 15 mL of hydrofluoric acid (HF; SIGMA-Aldrich), and then, the volume was adjusted to 500 mL using distilled water. The homogeneous solution was then stirred and heated at 40 °C. As a comparison, we also heated the solution at 80 °C for 2 h and performed the ultrasonication process for 2 h. The filtrate was used as a precursor solution to obtain W^{6+} in the subsequent reactions, and then, the solution was stored overnight prior to use.

Boric acid (H_3BO_3) was added to the W^{6+} precursor solutions with concentrations of 0.1, 0.2, 0.3, and 0.4 mol/mL, as shown in Figure 1b. A fluorine-doped tin oxide (FTO) (Bangkok Solar Co., Ltd., Thailand) electrode substrate with 2 × 3 cm^2 dimension was sonicated in a detergent for 10 min, 3 M NaOH for 30 min, ethanol and deionized water for 10 min, subsequently, and dried before the LPD reactions. The FTO substrate was immersed vertically in a 50 mL precursor solution and kept at 40 °C in a water bath for 6 h. After the deposition, the substrates were subsequently rinsed with distilled water and then calcined at 450 °C for 1 h.

2.2. Characterizations and Photoelectrochemical Measurements. X-ray diffraction (XRD; Rigaku, SmartLab) analyses were performed to examine the crystallinity of the fabricated FTO/WO_3 electrode. The morphologies and chemical compositions of the sample were investigated using scanning electron microscopy (SEM; JEOL, JSM −5410LV) and energy-dispersive X-ray spectroscopy (EDX; OXFORD, INCA-350). The oxidation states of deposits were evaluated using X-ray photoelectron spectroscopy (XPS, JEOL JPS-9010MC). The optical characters were examined using a UV−vis spectrophotometer (JASCO, V-7200). The PEC cell for the investigation of water oxidations consisted of FTO/WO_3, platinum wire (Pt), and Ag/AgCl (sat. KCl) as the working, counter, and reference electrodes, respectively. The efficiency of the WO_3 photoanode for water oxidation was evaluated by applying 1.0 V (vs Ag/AgCl) while subjecting it to 14.4-W light-emitting diode irradiation in a 0.5 M Na_2SO_4 electrolyte solution. The electrochemical characteristics of the WO_3 photoanode were investigated using cyclic voltammetry (CV) with the potential range and scan rate of −0.5 to 1.0 V and 50 mV s^{-1}, respectively. Electrochemical impedance spectroscopy (EIS) measurements were utilized to examine the electrochemical resistance, capacitance, and band state of the

https://doi.org/10.1021/acsomega.4c04738
ACS Omega 2024, 9, 38788−38797

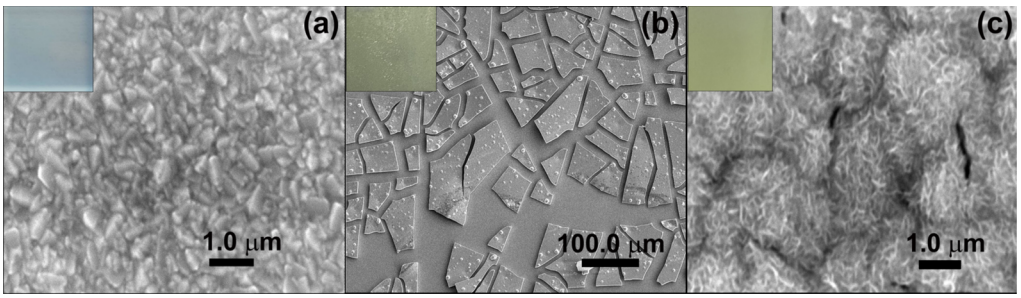

Figure 2. SEM images of (a) FTO and (b, c) FTO/WO_3 photoanodes fabricated by the LPD process. The precursor solutions were prepared at (b) 40 °C and (c) 80 °C, respectively.

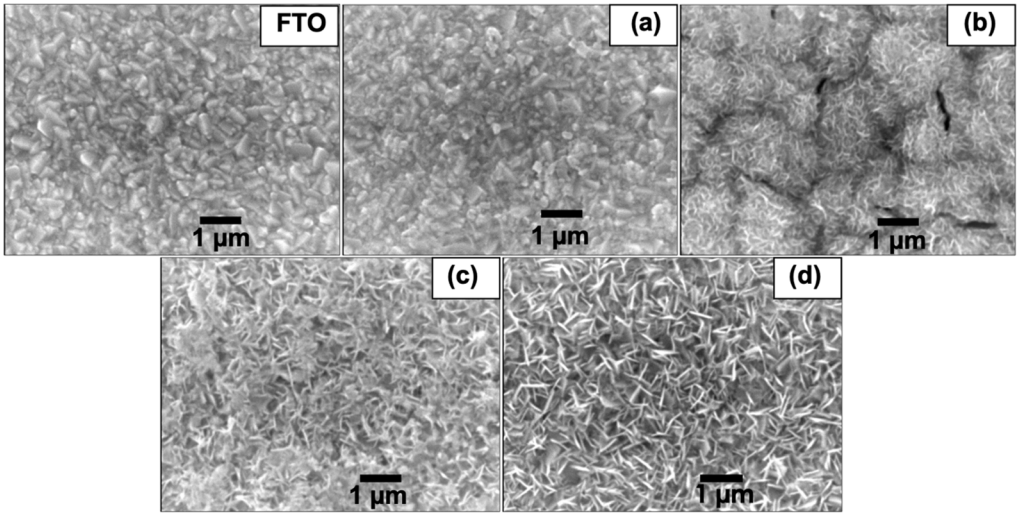

Figure 3. SEM images of the FTO and FTO/WO_3 photoanode prepared by the LPD method with concentrations of H_3BO_3 of (a) 0.1, (b) 0.2, (c) 0.3, and (d) 0.4 mol/mL.

fabricated WO_3 photoanode using a potentiostat (Princeton Applied Research, Inc., VersaSTAT3).

3. RESULTS AND DISCUSSION

3.1. Preparation Process of the WO_3 Precursor Solution. As shown in Figure 1a, the precursor solution became more homogeneous as the temperature was raised from 40 to 80 °C, indicating the impact of temperature on promoting the higher solubility of the tungstic precursor in the HF acid solvents. It was discovered that heating the precursor solution at 80 °C results in a clear yellow solution that was derived from $[WF_8]^{2-}$ and turns into a colorless $[W(OH)_8]^{2-}$ complex solution after the reaction was completed. At higher temperatures, tungstic acid (H_2WO_4) reacts with hydrofluoric acid to form a tungsten hexafluoride complex (H_2WF_8) with a faster reaction rate, facilitating the formation of the complex, as in eq 1. The tungsten hexafluoride complex $[WF_8]^{2-}$ reacts with H_2O to form a modified complex with hydroxide ligands and influences the kinetics of the reaction, as in eq 2. The modified complex reacts with additional H_2O, resulting in the formation of the $[W(OH)_8]^{2-}$ complex and affects the equilibrium of the reaction (eq 3).

$$H_2WO_4 + 8HF \rightarrow H_2WF_8 + 4H_2O \quad (1)$$

$$[WF_8]^{2-} + nH_2O \rightarrow [WF_{8-n}(OH)_n]^{2-} + nHF \quad (2)$$

$$[WF_{8-n}(OH)_n]^{2-} + nH_2O + (8-n)H_2O \leftrightarrow [W(OH)_8]^{2-} + (8-n)HF \quad (3)$$

The surface of the FTO substrate turned blue after the LPD process using a precursor solution containing a mixture of W^{6+} and H_3BO_3. The blue color on FTO glass is a result of a reduction in the oxidation state of tungsten from W^{6+} to W^{5+} by the H_3BO_3 at the FTO surface.[24,30−32] The LPD reaction process can be described as the following equations.

$$H_3BO_3 + 4HF \leftrightarrow BF^{4-} + H_3O^+ + 2H_2O \quad (4)$$

$$[W(OH_8)]^{2-} + 2H^+ \rightarrow WO_3 + 5H_2O \quad (5)$$

After the reaction, the thin WO_3 film with a yellow color was obtained by a calcination process in air at 450 °C for 1 h. The material's color changes from blue (W^{5+}) to yellow (W^{6+}) during the high-temperature treatment. To compare the effects of the precursor solution preparation temperatures, the characteristics of the WO_3 thin film obtained from the LPD process in both conditions were investigated, as shown in Figure 2. Figure 2b displays the FTO/WO_3 surfaces prepared by the precursor solution at 40 °C. Compared to Figure 2a (bare FTO), the depositions of WO_3 were confirmed in both cases. However, it was found that the precursor solution kept at 40 °C led to inhomogeneous depositions (having cracks) and lower adhesions, which can be easily peeled off. The insufficient adhesion of the thin film would be due to the incomplete reaction of H_2WO_3 and HF (eq 1) at a lower

https://doi.org/10.1021/acsomega.4c04738
ACS Omega 2024, 9, 38788−38797

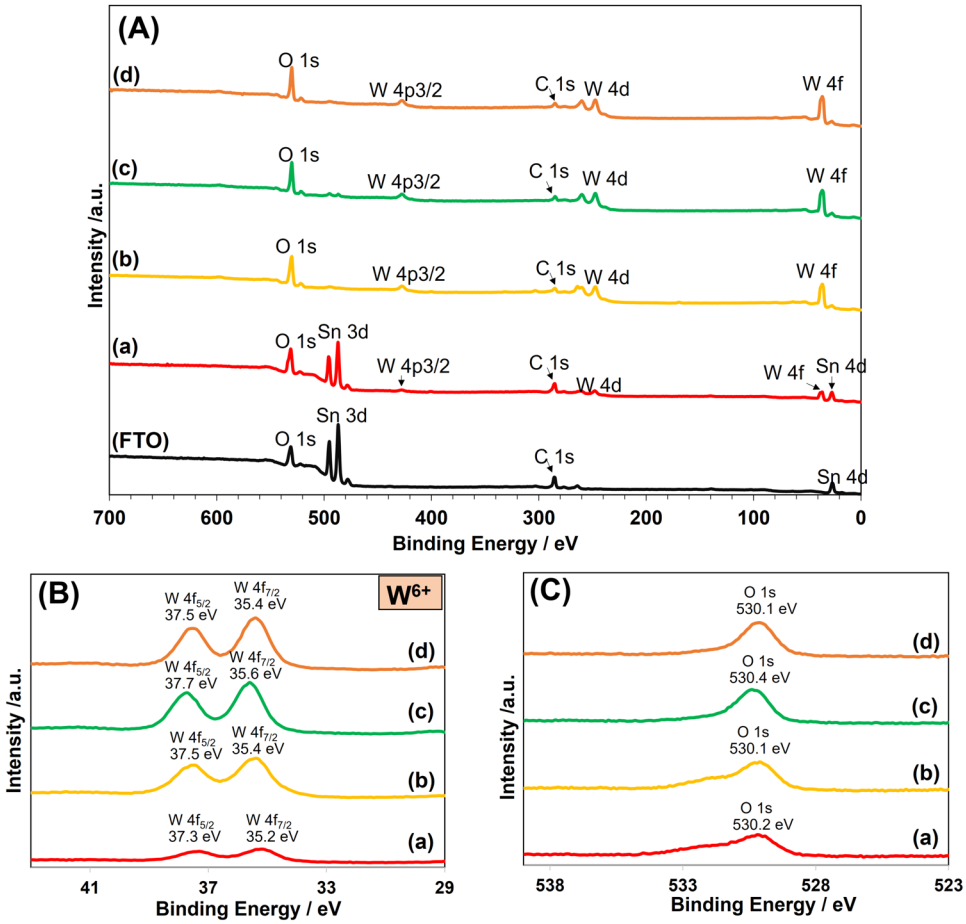

Figure 4. XPS spectra of (A) a wide scan of the WO_3 electrode compared with a narrow scan of (B) W_{4f} and (C) O 1s elements on the FTO/WO_3 electrode fabricated by the LPD method with concentrations of H_3BO_3 of (a) 0.1, (b) 0.2, (c) 0.3, and (d) 0.4 mol/mL.

temperature. From this, the complete hydroxylation of the tungsten hexafluoride complex (H_2WF_8) would lead to the incomplete conversion to $[W(OH)_8]^{2-}$ complex solution, as described in eqs 2 and 3. On the contrary, the FTO/WO_3 electrodes fabricated from the precursor solution prepared at 80 °C demonstrated a uniform, yellow, and smooth WO_3 film with the entire coverage of WO_3 (Figure 2c). The SEM image reveals a highly porous and rough surface. It can be expected that these morphologies would facilitate the photoanode activity due to the increased surface area, capacitance, and number of pathways for electron transfer. From this figure, since WO_3 covers the entire FTO glass surface, the electrode surface would be appropriate for photoelectrochemical measurements.

3.2. Effect of H_3BO_3 in the LPD Process for FTO/WO_3 Photoanode Fabrication. *3.2.1. Chemical Composition, Morphology, and Crystallinity.* The present study also evaluated the effect of the H_3BO_3 concentration in the precursor solution on the fabrication of WO_3 films. Figure 3 displays the top-view SEM images of FTO and FTO/WO_3 photoanodes prepared by the LPD method with varying concentrations of H_3BO_3. Figure 3a shows the FTO/WO_3 electrode surface prepared with a lower concentration of H_3BO_3 (0.1 mol/mL). From this result, it was found that a lower concentration of H_3BO_3 in the LPD process leads to fewer nucleation sites, resulting in insufficient WO_3 deposition. The lowest % weight of W was also obtained from the EDX data (Table S1 in the Supporting Information). Notably, the H_3BO_3 concentration in the precursor solution significantly affected the morphology of the WO_3 thin film at the electrode surface, as shown in Figure 3b–d. Especially under 0.2 mol/mL H_3BO_3 concentration conditions, small WO_3 nanoparticles are deposited uniformly on the surface, exhibiting high surface roughness and porosity. The obtained results demonstrate the function of H_3BO_3 in the production of WO_3 films in the LPD method, encompassing the influence on the crystal structure, morphology, and adhesion efficacy of the film to the electrode surface. Especially, Figure 3b exhibits the highest coverage of the WO_3 film under the H_3BO_3 concentration of 0.2 mol/mL. Thus, this finding, consistent with the highest weight % of W in EDX data (Table S1), indicates that the most suitable condition to control WO_3 adhesion by the LPD process is determined as the H_3BO_3 concentration of 0.2 mol/mL. This implies that the LPD technique is most effective for establishing a strong bond between WO_3 and a 0.2 mol/mL concentration. The strong adherence is due to enhanced chemical adhesion by the formation of boron–oxygen bonds at the boundary between the WO_3 film and the electrode. H_3BO_3 concentrations of 0.3 and 0.4 mol/mL diminish the adhesion effectiveness and coverage. This is because the abundant boron ions may occupy the reactive sites, reducing the quantity of WO_3 deposited and decreasing the film's homogeneity and adhesion. Conversely, the formation and deposition of WO_3 are not effectively supported when the concentration of boron ions is minimal, specifically, at 0.1 mol/mL. Consequently, there is a lack of adhesion and insufficient coverage. Therefore,

https://doi.org/10.1021/acsomega.4c04738
ACS Omega 2024, 9, 38788−38797

the structure and bonding of the WO_3 thin films are significantly influenced by the concentration of H_3BO_3. A 0.2 mol/mL concentration is optimal for attaining strong adhesion, high surface roughness, and homogeneous deposition, which leads to improved photoelectrochemical performance.

Figure 4A illustrates the wide-scan XPS spectra of the FTO/WO_3 electrode. The nanoparticles are composed of tungsten (W), oxygen (O), and carbon (C), as indicated by these spectra. The presence of these elements suggests that WO_3 has been effectively deposited onto the FTO substrate. The narrow scan XPS spectra of the W_{4f} region are depicted in Figure 4B. The W^{6+} oxidation state of WO_3 corresponds with the binding energies of the $W_{4f5/2}$ and $W_{4f7/2}$ peaks. The oxidation state of tungsten is unaffected by the varying concentrations of boric acid, as evidenced by the reason that these peaks remain consistent across all concentrations of H_3BO_3 used in the LPD process.[33−35] We employed deconvolutions to assess the oxidation states in the XPS spectra thoroughly. In the WO_3 composition, the analyzed spectra of W_{4f} verify the presence of W^{6+}. XPS spectra of the O_{1s} region are illustrated in Figure 4C, which offer insights into the oxidation state of oxygen in the crystalline WO_3.[36] Further validating the crystalline structure of the deposited WO_3, the deconvoluted O_{1s} spectra exhibit peaks associated with lattice oxygen and hydroxyl groups. In the article, the deconvoluted spectra and the observed binding energies agree with the previously reported values for WO_3. The chemical composition and oxidation state in the WO_3 electrode are carefully evaluated by analyzing high-resolution XPS spectra and including a wide-scan XPS spectrum.

In addition to SEM and XPS analyses, we performed XRD measurements of each substrate as shown in Figure 5. The

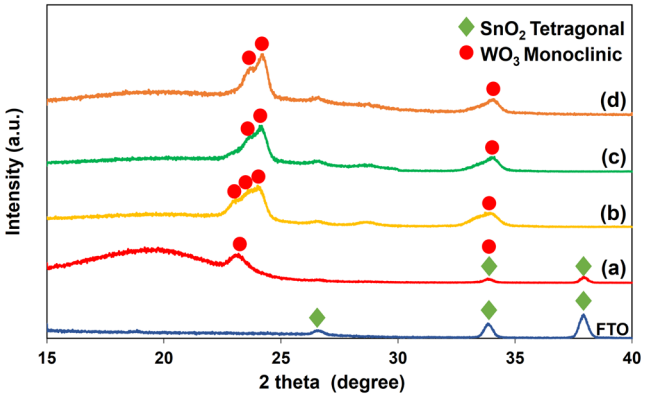

Figure 5. XRD patterns of FTO/WO_3 electrode fabrication using the LPD process at various H_3BO_3 concentrations of H_3BO_3 of (a) 0.1, (b) 0.2, (c) 0.3, and (d) 0.4 mol/mL.

tetragonal crystalline structure of SnO_2 derived from the FTO substrate was assigned to the peak at 2θ of 26.9, 34.1, and 38.8°.[37] From XRD patterns of the WO_3 film prepared with different H_3BO_3 concentrations, it was found that the variations in the concentration of H_3BO_3 affect the crystal structure of WO_3 at the surface of the electrodes (Figure 3a−d). Monoclinic WO_3 crystalline characteristics were observed as distinct XRD patterns at 23.1, 23.6, 24.4, and 34.1°,[38−40] while the boric acid concentration of 0.1 mol/mL exhibits distinct peaks at 2θ of 23.1 and 34.1°. The single broad peak at 23.1° would indicate the reduced crystallite's size and the crystallographic orientations under lower concentration conditions. When the concentration of H_3BO_3 increased from 0.2 to 0.4 mol/mL, clear XRD signals, corresponding to the high crystallinity of monoclinic WO_3, were obtained. This trend could be understood from eqs 4 and 5. The changes in H_3BO_3 amounts would lead to different amounts of proton source which accelerates eq 5. In other words, the inappropriate ratio of H_3BO_3 would induce the reverse reaction in eqs 4 and 5, providing low crystallinity or a small deposition of monoclinic WO_3. These findings suggest that an appropriate concentration of H_3BO_3 can enhance the growth of specific crystallographic phases or orientations, resulting in an enhanced crystalline quality of WO_3 on the FTO substrate.

3.2.2. Optical Properties Effect. The effect of H_3BO_3 concentration on the optical properties of the prepared films was evaluated, as shown in Figure 6. The highest visible light

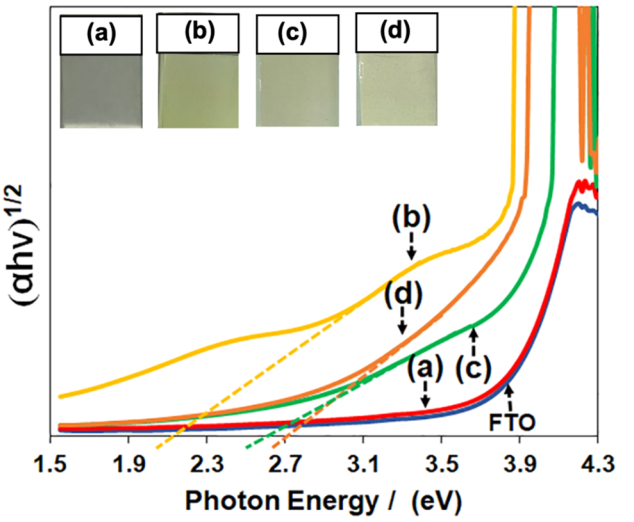

Figure 6. Absorption spectra of the FTO substrate and FTO/WO_3 photoanode fabricated by the LPD process with various concentrations of H_3BO_3 in precursor solution as (a) 0.1, (b) 0.2, (c) 0.3, and (d) 0.4 mol/mL.

absorption properties of the FTO/WO_3 electrode were obtained when fabricated at an H_3BO_3 concentration of 0.2 mol/mL, as indicated by the highest WO_3 content and in good relation to the darkest yellow color of the WO_3 semiconductor,[41−43] as shown in the insets of Figure 6. When the concentration of H_3BO_3 in the LPD process was increased to 0.3 and 0.4 mol/mL, the prepared WO_3 electrode exhibited decreased visible light absorption and a light-yellow color. The high concentration of H_3BO_3 could cause a decrease in the amount of WO_3 on the electrode surface. This would be attributed to the saturation of active sites by the presence of boron ions, leading to inadequate adhesion and the changes in the electronic state. In the opposite direction, under the lowest H_3BO_3 concentration of 0.1 mol/mL, the WO_3 film is colorless and lacks visible light absorption properties, indicating a very low WO_3 level at the electrode surface. This effect occurs because the lowest concentration of H_3BO_3 is insufficient to promote the formation of the WO_3 film through the LPD process. The band gap energy (E_g) was determined using Tauc's eq (eq 6), which was calculated using the following equation

$$\alpha h\nu = A(h\nu - E_g)^{1/2} \quad (6)$$

https://doi.org/10.1021/acsomega.4c04738
ACS Omega 2024, 9, 38788−38797

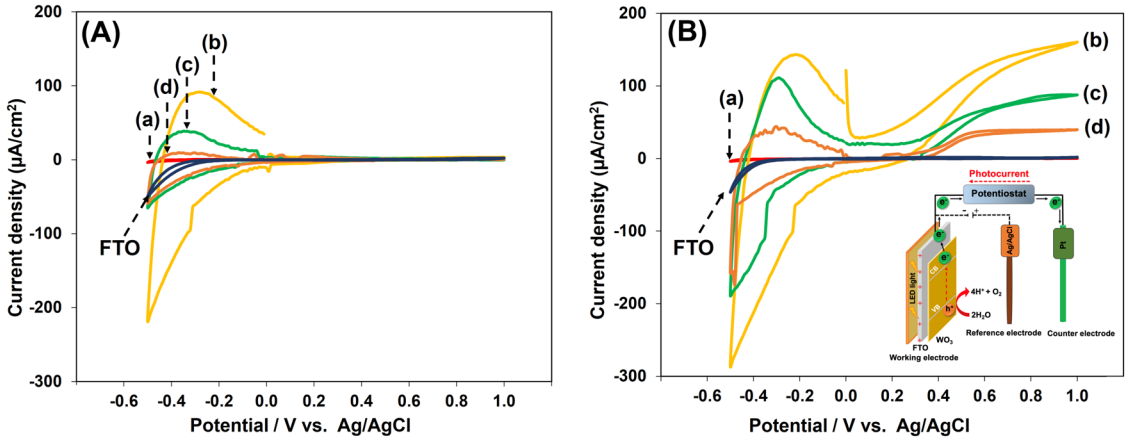

Figure 7. Cyclic voltammograms of the FTO/WO_3 electrode fabricated by the LPD method with varying H_3BO_3 concentrations of (a) 0.1, (b) 0.2, (c) 0.3, and (d) 0.4 mol/mL under (A) dark and (B) visible light irradiation conditions. The potential scan rate and supporting electrolyte were 50 mV s^{-1} and 0.5 M Na_2SO_4.

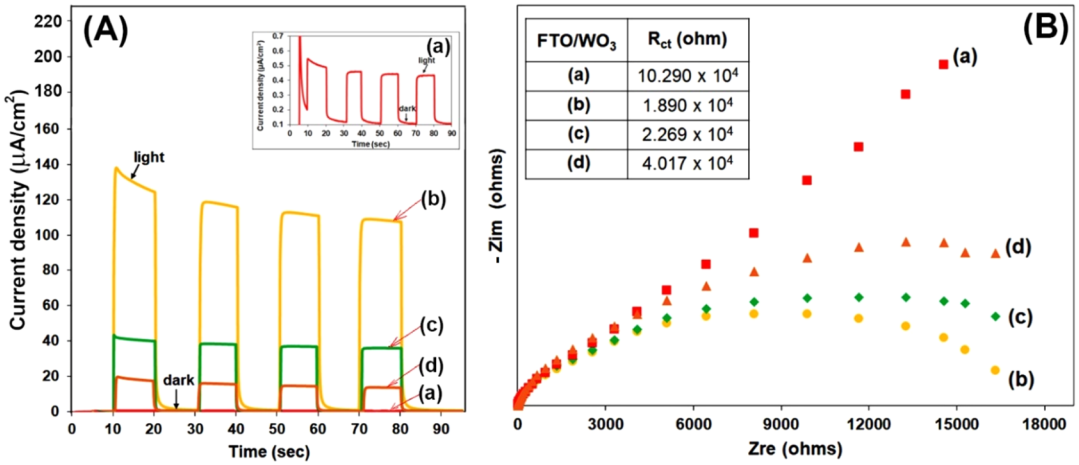

Figure 8. (A) Photocurrent from water oxidation and (B) Nyquist plots of the FTO/WO_3 photoanode fabricated by the LPD process with concentrations of H_3BO_3 of (a) 0.1, (b) 0.2, (c) 0.3, and (d) 0.4 mol/mL at the static potential of 1.0 V vs Ag/AgCl under visible light illuminations. The electrolyte was a 0.5 M Na_2SO_4 aqueous solution. The inset in (B) is the charge transfer rate (R_{ct}) values for each electrode.

where α, $h\nu$, A, and E_g are the absorption coefficient, photon energy, a constant, and the calculated bad gap energy, respectively. Figure 6 shows the spectra of $(\alpha h\nu)^{1/2}$ against the photon energy. From this figure, it was found that the band gap energy for the prepared film ranged between 2.1 and 2.8 eV. Particularly, the optimal condition for WO_3 photoanode fabrication demonstrates the narrowest band gap energy at 2.1 eV due to an appropriate H_3BO_3 concentration that can facilitate nucleation and well-adhesion on the substrate. This corresponds with the highest weight percent of W in the EDX data of FTO/WO_3 electrodes, which causes the electrodes to display the darkest yellow color, resulting in the highest visible light absorption properties. The different band gap energies would be derived from the different oxygen contents or the defect sites, which provide the additional energy states. Thus, it was found that the concentration of H_3BO_3 affected not only the surface morphology and deposited amounts but also the electronic structure of WO_3 through the changes in the boron species amounts. To summarize, the concentration of H_3BO_3 has a significant impact on the properties of a WO_3 thin film, including how it starts, grows, shapes, crystallizes, has flaws, and looks. These variables collectively influence band gap energy changes. An optimal concentration of H_3BO_3 improves these characteristics, leading to the highest photoelectrochemical efficiency and band gap energy.

3.2.3. Photoelectrocatalytic Activities. For the investigations of photoelectrochemical properties of prepared WO_3 films, the CV measurements were conducted in an aqueous solution under various applied electrochemical potentials and visible light illuminations (λ_{ex} = 420−680 nm). Figure 7 shows the oxidation and reduction currents obtained with the potential range between −0.5 and 1.0 V under dark or light illumination conditions. The current values exhibited a linear relationship with the amount of WO_3 deposited on the FTO substrate in both light and dark conditions, related to the effect of H_3BO_3 concentration during the FTO/WO_3 electrode fabrication processes. The current values within this potential range can quantitatively confirm the formation of the WO_3 film under each condition and support the findings of the EDX analyses.[44] Due to the lack of any sacrificial agent in the aqueous solution, Figure 7B confirms the occurrence of the photoelectrocatalytic water oxidations at the FTO/WO_3 photoanode even under the neutral solution condition (as in the inset of Figure 7B). The FTO/WO_3 photoanode prepared from H_3BO_3 at a concentration of 0.2 mol/mL exhibits the highest photoelectrocatalytic activity for water oxidation.

https://doi.org/10.1021/acsomega.4c04738
ACS Omega 2024, 9, 38788−38797

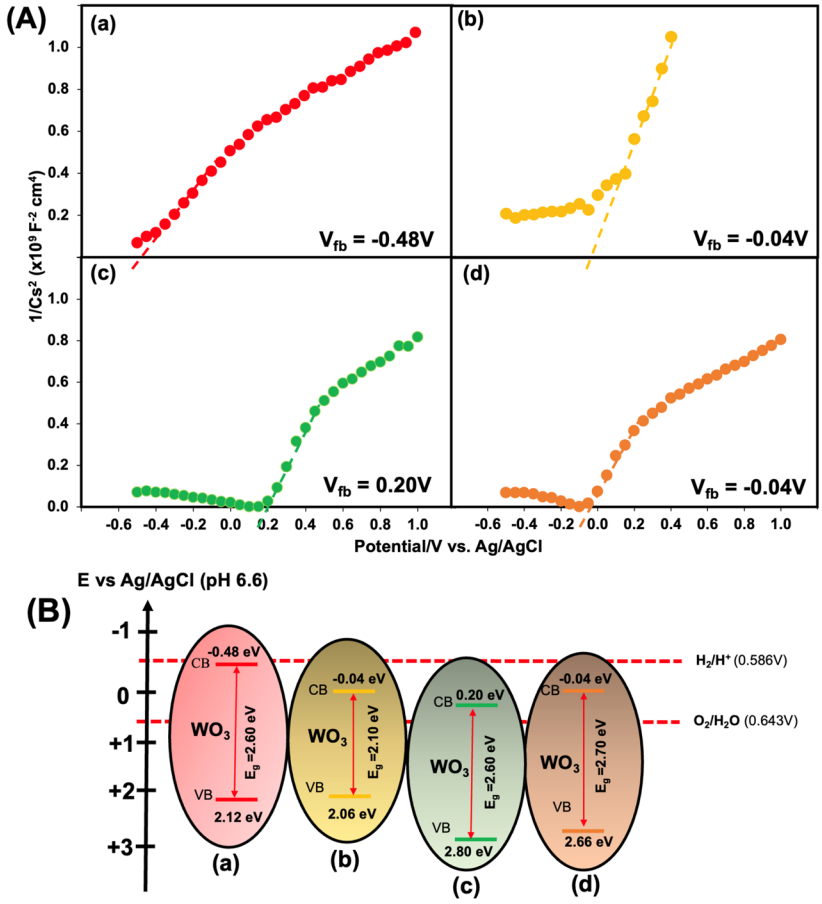

Figure 9. (A) Mott−Schottky plots and Φ_{fb} values for each electrode obtained at a frequency of 10,000 Hz. (B) Energy band diagrams of FTO/WO_3 fabricated by the LPD process with various H_3BO_3 concentrations of (a) 0.1, (b) 0.2, (c) 0.3, and (d) 0.4 mol/mL.

Under this condition, the onset potential for water oxidation begins at 0.1 V and is more negative than under other conditions, indicating that the electrocatalytic activity of the electrode was promoted. Under the light illuminations, the light-stimulating WO_3 semiconductor causes the separation of electron (e^-) and hole (h^+) excited from the VB to the conduction band (CB). The generated e^- at CB is transferred to the counter electrode, while the remaining h^+ at VB oxidizes the H_2O at the electrode surface to produce oxygen. While under dark conditions, as shown in Figure 7A, no evidence was found that the water oxidation peak was caused by the absence of light illuminations.

Figure 8A demonstrates that the photoelectrocatalytic activity of the FTO/WO_3 photoanode for water oxidation was dependent on the H_3BO_3 concentrations in the LPD process by using a conventional three-electrode system under on−off light illuminations. This result indicates that a suitable concentration of H_3BO_3 can facilitate the strong adhesion of the WO_3 thin film to the substrate, which improves the photoelectrocatalytic activity of the FTO/WO_3 electrodes. The repetitive light illuminations at the constant potential also showed this tendency, as shown in Figure 8A. Moreover, the EIS measurements were utilized to investigate the charge transfer resistance (R_{ct}) of the FTO/WO_3 photoanode fabricated by varying concentrations of H_3BO_3 in the LPD process. Figure 8B demonstrates that FTO/WO_3 fabricated at an H_3BO_3 concentration of 0.2 mol/mL has the smallest semicircle of the Nyquist plot, corresponding to the lowest value of charge transfer resistance (R_{ct}) compared to other conditions. The lowest R_{ct} value under the optimal conditions implies the highest electron transfer rate at the electrode surface, which is in good agreement with the highest photocurrent generations. The research demonstrates that the concentration of H_3BO_3 in the precursor solution has a substantial influence on the photoelectrocatalytic activity of the FTO/WO_3 photoanode produced via the LPD approach. Boric acid is a critical factor in forming and enlarging WO_3 crystals, which impacts the films' adhesion, shape, and arrangement via the LPD method. Our research reveals that a boric acid concentration of 0.2 mol/mL produces WO_3 coatings in a highly uniform and highly crystalline state. As a result of their robust adhesion to the FTO substrate, these coatings improve light absorption and charge separation. Conversely, films produced at concentrations that are either higher or lower are less effective, as a result of insufficient nucleation or excessive saturation. Following the reaction with boric acid, it is possible to modify the residual HF in order to generate a fully integrated W-fluoride complex. It is essential to achieve a well-defined crystalline structure and robust adhesion in order to enhance reactivity and optimize the surface area.

3.2.4. Electronic Structure of Deposited Films. Mott−Schottky (MS) curves were utilized to verify the positions of the CB energy (Φ_{CB}) or flat band potentials (Φ_{fb}) of the WO_3 thin film under the dark condition. Figure 9A demonstrates that all samples showed the n-type semiconductor properties as can be found from the positive slope.[45,46] The Φ_{fb} values for

https://doi.org/10.1021/acsomega.4c04738
ACS Omega 2024, 9, 38788−38797

Table 1. Comparison of Current Densities for WO_3 Photoanodes by Different Fabrication Methods

photoanode	fabrication process	electrolyte/light source	current density at 1.00 V vs Ag/AgCl	ref
FTO/WO_3	LPD	0.5 M Na_2SO_4/14.4-W light-emitting diode (LED)	∼120 μAcm^{-2} at	this work
FTO/WO_3/Fe_2O_3	sputtering	0.5 M Na_2SO_4/visible light irradiation	∼50 μAcm^{-2}	47
ITO/WO_3	FPD	0.1 M Na_2SO_4/60-W tungsten lamp	∼80 μAcm^{-2}	41
ITO/WO_3	electrodeposition	0.1 M Na_2SO_4/visible light illuminated	∼90 μAcm^{-2}	42

each electrode were found to be at −0.48, −0.040, 0.20, and −0.040 V vs Ag/AgCl, respectively, when the H_3BO_3 concentration was varied to 0.1, 0.2, 0.3, and 0.4 mol/mL. From these values, the energy level of the valence band (Φ_{VB}) position of each FTO/WO_3 could be determined using the following equation as $\Phi_{fb} = \Phi_{CB} + E_g$. The Φ_{VB} values for FTO/WO_3 under different concentrations of H_3BO_3 of 0.1, 0.2, 0.3, and 0.4 mol/mL are found to be 2.12, 2.06, 2.80, and 2.66 V (vs Ag/AgCl), respectively. Such a difference would also originate from the different oxygen contents, defect sites at the band gap, or fluorine contents. This is supported by the different slopes of MS plots, which reflect the doping density of the semiconductor.

Figure 9B depicts a schematic energy diagram of the electronic structure of fabricated WO_3 depending on the H_3BO_3 concentration. It verifies that the optimal electronic band structure for photoelectrocatalytic water oxidation under visible light irradiation is exhibited by the FTO/WO_3 photoanode prepared with a 0.2 mol/mL H_3BO_3 condition. It displays the narrowest band gap energy value, leading to the highest visible light absorption properties and highest photocurrent values. Furthermore, it was observed that the VB of WO_3 was more positive than the water oxidation potential in all situations, verifying its capacity to convert water oxidation into oxygen. The findings validate that WO_3 electrodes, prepared with a boric acid concentration of 0.2 mol/mL, exhibit maximum photocurrent. This is attributed to their exceptional light absorption capability and superior h^+ production, enhancing the water oxidation efficiency. It is evident from the aforementioned statement that the concentration of H_3BO_3 in the precursor solution substantially influences the characteristic and photoelectrocatalytic activity of the FTO/WO_3 photoanodes. The function of H_3BO_3 in the precursor solution for WO_3 film fabrication in the LPD process is to regulate the amount of HF that remains after the reaction, which promotes the formation of a fully integrated W-fluoride complex compound. This compound production process significantly affects the WO_3 thin film's effective adhesion to the FTO substrate. The effective optimization of H_3BO_3 concentration in the LPD method facilitates achieving excellent adhesion efficiency for the WO_3 film. This is supported by developing an well-defined crystalline structure, distinctive morphology with a substantial surface area for enhanced reactivity, and the capacity to exhibit desirable properties. The exceptional capacity of WO_3 to efficiently absorb visible light is attributed to its favorable electrical band structure. The outcome of this study yields a WO_3 photoanode with exceptional photoelectrocatalytic water oxidation characteristics. Moreover, it should be emphasized that the present improvements in current density are notable when we compare the photoconversion abilities with other fabrication processes, as can be found in Table 1.[47] From the above facts, it is possible to conclude that our current electrode preparation procedure would be a promising candidate for future advancements in energy and environmental management applications.

4. CONCLUSIONS

A highly homogeneous precursor solution with a large volume was successfully produced for the fabrication of a WO_3 photoanode using the LPD technique. It can reduce inconsistencies, save time, and facilitate the LPD process for fabricating WO_3 thin films. The utilization of boric acid in the LPD process has a notable impact on the development of WO_3 thin films, particularly in enhancing their adhesion to the electrode substrate. The optimal WO_3 thin film production condition is a 0.2 mol/mL concentration of H_3BO_3 in the precursor solution, which results in various desirable properties. These characteristics include a high current density, low charge transfer resistance, high surface roughness, and good crystallinity. Furthermore, it exhibits a great capacity for absorbing visible light due to its appropriate band energy, hence demonstrating exceptional photoelectrocatalytic characteristics for water oxidation. The findings of this study demonstrate that the WO_3 photoanode prepared by the present procedure has remarkable photoelectrocatalytic water oxidation properties, establishing it as a prospective contender for future developments in energy and environmental management applications.

■ ASSOCIATED CONTENT

Supporting Information

The Supporting Information is available free of charge at https://pubs.acs.org/doi/10.1021/acsomega.4c04738.

Energy-dispersive X-ray analyses of the synthesized films shown in Figure 3 (PDF)

■ AUTHOR INFORMATION

Corresponding Authors

Chatchai Ponchio − *Department of Chemistry, Faculty of Science and Technology, Rajamangala University of Technology Thanyaburi, Thanyaburi, Pathum Thani 12120, Thailand; Advanced Photochemical and Electrochemical Materials (APEM) Research Unit, Faculty of Science and Technology, Rajamangala University of Technology Thanyaburi, Khlong Hok, Pathum Thani 12110, Thailand*; Email: chatchai@rmutt.ac.th

Hiro Minamimoto − *Department of Chemical Science and Engineering, Graduate School of Engineering, Kobe University, Nada-ku, Kobe 657-8501, Japan*; orcid.org/0000-0002-2360-577X; Email: minamimoto@godzilla.kobe-u.ac.jp

Authors

Watcharapong Nareejun − *Department of Chemistry, Faculty of Science and Technology, Rajamangala University of Technology Thanyaburi, Thanyaburi, Pathum Thani 12120, Thailand*

https://doi.org/10.1021/acsomega.4c04738
ACS Omega 2024, 9, 38788−38797

Minoru Mizuhata − *Department of Chemical Science and Engineering, Graduate School of Engineering, Kobe University, Nada-ku, Kobe 657-8501, Japan;* orcid.org/0000-0002-4496-2215

Complete contact information is available at: https://pubs.acs.org/10.1021/acsomega.4c04738

Notes

The authors declare no competing financial interest.

■ ACKNOWLEDGMENTS

This work was supported by the Research and Researchers for Industries (RRI) project and Eagle dream Co., Ltd. (N41A650408). The JSPS KAKENHI (JP22K144960 and JP22K18315) from the Ministry of Education, Culture, Sports, Science, and Technology of Japan, Nippon Sheet Glass Foundation, Kansai Research Foundation for technology promotion is also acknowledged.

■ REFERENCES

(1) Mesones, S.; Mena, E.; López-Muñoz, M. J.; Adán, C.; Marugán, J. Synergistic and antagonistic effects in the photoelectrocatalytic disinfection of water with TiO_2 supported on activated carbon as a bipolar electrode in a novel 3D photoelectrochemical reactor. *Sep. Purif. Technol.* **2020**, *247*, 117002.

(2) Zhang, J.; Tang, B.; Zhao, G. Selective photoelectrocatalytic removal of dimethyl phthalate on high-quality expressed molecular imprints decorated specific facet of single crystalline TiO_2 photoanode. *Appl. Catal. B: Environ.* **2020**, *279*, 119364.

(3) Mu, F.; Dai, B.; Zhao, W.; Zhang, L.; Xu, J.; Guo, X. A review on metal-organic frameworks for photoelectrocatalytic applications. *Chin. Chem. Lett.* **2020**, *31* (7), 1773−1781.

(4) Shao, Z.; Zhang, Y.; Yang, X.; Zhong, M. Au-Mediated Charge Transfer Process of Ternary Cu_2O/Au/TiO2-NAs Nanoheterostructures for Improved Photoelectrochemical Performance. *ACS Omega* **2020**, *5* (13), 7503−7518.

(5) Srevarit, W.; Moonmangmee, S.; Phapugrangkul, P.; Kuboon, S.; Klamchuen, A.; Saito, N.; Ponchio, C. Photoelectrocatalytic H2 evolution enhancement over CuO-decorated TiO_2 nanocatalysts and promoting E. coli degradation. *J. Alloys Compd.* **2021**, *859*, 157818.

(6) Rojviroon, T.; Laobuthee, A.; Sirivithayapakorn, S. Photocatalytic Activity of Toluene under UV-LED Light with TiO_2 Thin Films. *Int. J. Photoenergy* **2012**, *2012* (1), 1−8.

(7) Tayebi, M.; Lee, B.-K. Recent advances in $BiVO_4$ semiconductor materials for hydrogen production using photoelectrochemical water splitting. *Renewable Sustainable Energy Rev.* **2019**, *111*, 332−343.

(8) Zhou, S.; Yue, P.; Huang, J.; Wang, L.; She, H.; Wang, Q. High-performance photoelectrochemical water splitting of $BiVO_4$@Co-MIm prepared by a facile in-situ deposition method. *Chem. Eng. J.* **2019**, *371*, 885−892.

(9) Bemana, H.; Rashid-Nadimi, S. Incorporation of NiO electrocatalyst with α-Fe_2O_3 photocatalyst for enhanced and stable photoelectrochemical water splitting. *Surf. Interfaces* **2019**, *14*, 184−191.

(10) Farooq, U.; Chaudhary, P.; Ingole, P. P.; Kalam, A.; Ahmad, T. Development of Cuboidal $KNbO_3$@α-Fe_2O_3 Hybrid Nanostructures for Improved Photocatalytic and Photoelectrocatalytic Applications. *ACS Omega* **2020**, *5* (32), 20491−20505.

(11) Mansoor, M. A.; Munawar, K.; Naeem, R.; Sarih, N. M.; Asghar, M. A.; Haider, A.; Zubir, M. N. M.; Zaharinie, T. Aerosol-assisted facile fabrication of bimetallic Cr_2O_3-Mn_2O_3 thin films for photoelectrochemical water splitting. *New J. Chem.* **2023**, *47* (17), 8347−8354.

(12) Ahmed, S.; Mansoor, M. A.; Basirun, W. J.; Sookhakian, M.; Huang, N. M.; Mun, L. K.; Söhnel, T.; Arifin, Z.; Mazhar, M. The synthesis and characterization of a hexanuclear copper-yttrium complex for deposition of semiconducting $CuYO_2$-0.5Cu_2O composite thin films. *New J. Chem.* **2015**, *39*, 1031−1037.

(13) Naeem, R.; Mansoor, M. A.; Munawar, K.; Adnan, A.; Zaharinie, T.; Mohd Zubir, M. N. Versatile Fabrication of Binary Composite SnO_2-Mn_2O_3 Thin Films by AACVD for Synergistic Photocatalytic Effect. *J. Electron. Mater.* **2021**, *50* (7), 3897−3906.

(14) Chatchai, P.; Murakami, Y.; Kishioka, S.-y.; Nosaka, A. Y.; Nosaka, Y. Efficient photocatalytic activity of water oxidation over WO_3/$BiVO_4$ composite under visible light irradiation. *Electrochim. Acta* **2009**, *54* (3), 1147−1152.

(15) Peleyeju, G. M.; Umukoro, E. H.; Babalola, J. O.; Arotiba, O. A. Solar-Light-Responsive Titanium-Sheet-Based Carbon Nanoparticles/B-$BiVO_4$/WO_3 Photoanode for the Photoelectrocatalytic Degradation of Orange II Dye Water Pollutant. *ACS Omega* **2020**, *5* (10), 4743−4750.

(16) Tayebi, M.; Masoumi, Z.; Lee, B.-K. Ultrasonically prepared photocatalyst of W/WO_3 nanoplates with WS_2 nanosheets as 2D material for improving photoelectrochemical water splitting. *Ultrason. Sonochem.* **2021**, *70*, 105339.

(17) Seferlis, A. K.; Neophytides, S. G. On the kinetics of photoelectrocatalytic water splitting on nanocrystalline TiO_2 films. *Appl. Catal., B* **2013**, *132*−*133*, 543−552.

(18) Nomellini, C.; Polo, A.; Mesa, C. A.; Pastor, E.; Marra, G.; Grigioni, I.; Dozzi, M. V.; Giménez, S.; Selli, E. Improved Photoelectrochemical Performance of WO_3/$BiVO_4$ Heterojunction Photoanodes via WO_3 Nanostructuring. *ACS Appl. Mater. Interfaces* **2023**, *15* (45), 52436−52447.

(19) Naeem, R.; Afzal, S.; Mansoor, M. A.; Munawar, K.; Sherino, B.; Ahmed, R. A composite approach to synthesize a high-performance Pt/WO_3-carbon catalyst for optical and electrocatalytic applications. *New J. Chem.* **2022**, *46* (28), 13454−13464.

(20) Kangkun, N.; Ponchio, C. Photoelectrodeposition of $BiVO_4$ layer on FTO/WO_3 photoanodes for highly efficient photoelectrocatalytic chemical oxygen demand sensor applications. *Appl. Surf. Sci.* **2020**, *526*, 146686.

(21) Limwichean, S.; Kasayapanand, N.; Ponchio, C.; Nakajima, H.; Patthanasettakul, V.; Eiamchai, P.; Meng, G.; Horprathum, M. Morphology-controlled fabrication of nanostructured WO_3 thin films by magnetron sputtering with glancing angle deposition for enhanced efficiency photo-electrochemical water splitting. *Ceram. Int.* **2021**, *47* (24), 34455−34462.

(22) Chatchai, P.; Nosaka, A. Y.; Nosaka, Y. Photoelectrocatalytic performance of WO_3/$BiVO_4$ toward the dye degradation. *Electrochim. Acta* **2013**, *94*, 314−319.

(23) Deki, S.; Yu Yu Ko, H.; Fujita, T.; Akamatsu, K.; Mizuhata, M.; Kajinami, A. Synthesis and microstructure of metal oxide thin films containing metal nanoparticles by liquid phase deposition (LPD) method. *Eur. Phys. J. D* **2001**, *16* (1), 325−328.

(24) Zhang, M.; Yang, C.; Pu, W.; Tan, Y.; Yang, K.; Zhang, J. Liquid phase deposition of WO_3/TiO_2 heterojunction films with high photoelectrocatalytic activity under visible light irradiation. *Electrochim. Acta* **2014**, *148*, 180−186.

(25) Yamanaka, S.; Hamaguchi, T.; Muta, H.; Kurosaki, K.; Uno, M. Fabrication of oxide nanohole arrays by a liquid phase deposition method. *J. Alloys Compd.* **2004**, *373* (1−2), 312−315.

(26) Saito, Y.; Sekiguchi, Y.; Mizuhata, M.; Deki, S. Continuous Deposition System of SnO_2 Thin Film by the Liquid Phase Deposition (LPD) Method. *J. Ceram. Soc. Jpn.* **2007**, *115*, 856−860.

(27) Mizuhata, M. Aqueous solution reaction during liquid-phase deposition and its application in electrochemical materials. *J. Ceram. Soc. Jpn.* **2022**, *130* (9), 752−761.

(28) Huang, J.-J.; Lin, C.-H.; Ho, Y.-R.; Chang, Y.-H. Aluminium oxide passivation films by liquid phase deposition for TiO_2 ultraviolet solid-liquid heterojunction photodetectors. *Surf. Coat. Technol.* **2020**, *391*, 125684.

(29) Lei, P.-H.; Ding, M.-J.; Lee, Y.-C.; Chung, M.-J. Textured zinc oxide prepared by liquid phase deposition (LPD) method and its application in improvement of extraction efficiency for 650nm

resonant-cavity light-emitting diode (RCLED). *J. Alloys Compd.* **2011**, *509* (21), 6152−6157.
(30) Mohammad-Hosseinpour, M.; Yourdkhani, A.; Poursalehi, R. Fast-switching electrochromic response of $WO_3{\cdot}2H_2O$ of plate-like particles synthesized by liquid phase deposition. *J. Alloys Compd.* **2021**, *879*, 160418.
(31) Deki, S.; Béléké, A. B.; Kotani, Y.; Mizuhata, M. Synthesis of tungsten oxide thin film by liquid phase deposition. *Mater. Chem. Phys.* **2010**, *123* (2), 614−619.
(32) Darmawi, S.; Burkhardt, S.; Leichtweiss, T.; Weber, D.; Wenzel, S.; Janek, J.; Elm, M.; Klar, P. Correlation of electrochromic properties and oxidation states in nanocrystalline tungsten trioxide. *Phys. Chem. Chem. Phys.* **2015**, *17*, 15903−15911.
(33) Nareejun, W.; Ponchio, C. Novel photoelectrocatalytic/solar cell improvement for organic dye degradation based on simple dip coating $WO_3/BiVO_4$ photoanode electrode. *Sol. Energy Mater. Sol. Cells* **2020**, *212*, 110556.
(34) Ji, R.; Zheng, D.; Zhou, C.; Cheng, J.; Yu, J.; Li, L. Low-Temperature Preparation of Tungsten Oxide Anode Buffer Layer via Ultrasonic Spray Pyrolysis Method for Large-Area Organic Solar Cells. *Materials (Basel)* **2017**, *10* (7), 820.
(35) Yao, J. N.; Chen, P.; Fujishima, A. Electrochromic behavior of electrodeposited tungsten oxide thin films. *J. Electroanal. Chem.* **1996**, *406* (1−2), 223−226.
(36) Leftheriotis, G.; Papaefthimiou, S.; Yianoulis, P.; Siokou, A. Effect of the tungsten oxidation states in the thermal coloration and bleaching of amorphous WO_3 films. *Thin Solid Films* **2001**, *384* (2), 298−306.
(37) Yu, H.; Yang, T.; Wang, Z.; Li, Z.; Zhao, Q.; Zhang, M. p-N heterostructural sensor with $SnO\text{-}SnO_2$ for fast NO_2 sensing response properties at room temperature. *Sens. Actuators, B* **2018**, *258*, 517−526.
(38) Kumbhar, V. S.; Lee, H.; Lee, J.; Lee, K. Interfacial growth of the optimal $BiVO_4$ nanoparticles onto self-assembled WO_3 nanoplates for efficient photoelectrochemical water splitting. *J. Colloid Interface Sci.* **2019**, *557*, 478−487.
(39) Castillo, C.; Cabello, G.; Chornik, B.; Huentupil, Y.; Buono-Core, G. E. Characterization of photochemically grown Pd loaded WO_3 thin films and its evaluation as ammonia gas sensor. *J. Alloys Compd.* **2020**, *825*, 154166.
(40) Choi, J.; Song, T.; Kwon, J.; Lee, S.; Han, H.; Roy, N.; Terashima, C.; Fujishima, A.; Paik, U.; Pitchaimuthu, S. WO_3 nanofibrous backbone scaffolds for enhanced optical absorbance and charge transport in metal oxide (Fe_2O_3, $BiVO_4$) semiconductor photoanodes towards solar fuel generation. *Appl. Surf. Sci.* **2018**, *447*, 331−337.
(41) Kangkun, N.; Kiama, N.; Saito, N.; Ponchio, C. Optical properties and photoelectrocatalytic activities improvement of WO_3 thin film fabricated by fixed-potential deposition method. *Optik* **2019**, *198*, 163235.
(42) Supanantin, F.; Ponchio, C. Improvement ITO/WO_3 photo anode electrode fabrication using electrodeposition technique for highly efficient photoelectrocatalytic insecticide degradation. *Mater. Sci. Semicond. Process.* **2020**, *118*, 105212.
(43) Bi, Q.; Gao, Y.; Wang, Z.; Dang, C.; Zhang, Z.; Wang, L.; Xue, J. Preparation of a direct Z-scheme thin-film electrode based on CdS QD-sensitized $BiOI/WO_3$ and its photoelectrocatalytic performance. *Colloids Surf., A* **2020**, *599*, 124849.
(44) Xie, H.; Wang, Y.; Liu, H.; Wang, H.; Li, Y.; Qi, X.; Liang, T.; Zeng, J. Electrochromic electrode with high optical contrast and long cyclic life using nest-like porous doped-Sm WO_3 films. *Ceram. Int.* **2023**, *49* (5), 8223−8231.
(45) Ba, G.; Liang, Z.; Li, H.; Du, N.; Liu, J.; Hou, W. Simultaneous formation of mesopores and homojunctions in graphite carbon nitride with enhanced optical absorption, charge separation and photocatalytic hydrogen evolution. *Appl. Catal. B: Environ.* **2019**, *253*, 359−368.
(46) Yan, K.; Liu, J.; Qin, J.; Zhang, J. A portable solar light-driven biophotoelectrocatalytic system for pollutant removal powered by photovoltaic cells. *J. Hazard. Mater.* **2022**, *435*, 128989.
(47) Wiriyachailerd, C.; Horprathum, M.; Eiamchai, P.; Ponchio, C. Improved the charge transfer for highly efficient photoelectrochemical water oxidation: the case of WO_3 and $BiVO_4$. *Mater. Today: Proc.* **2018**, *5* (6), 13874−13878.

https://doi.org/10.1021/acsomega.4c04738
ACS Omega 2024, 9, 38788−38797